Materials Today Physics 55 (2025) 101758

Contents lists available at ScienceDirect

Materials Today Physics

journal homepage: www.journals.elsevier.com/materials-today-physics

Boosted energy harvesting performance of magneto-mechano-electric generator via photon flash annealing for self-powered IoT sensors

Hyunseok Song [a,1], Srinivas Pattipaka [b,1], Yun Sik Hwang [c], Mahesh Peddigari [d], Yuho Min [e], Kyeongwoon Chung [f], Jung Hwan Park [c], Chang Kyu Jeong [g], Han Eol Lee [g], Jongmoon Jang [h], Kwi-Il Park [e], Sung-Dae Kim [a], Jaewon Jeong [i], Woon-Ha Yoon [i], Jungho Ryu [a,*], Geon-Tae Hwang [b,**]

[a] School of Materials Science and Engineering, Yeungnam University, 280 Daehak-ro, Gyeongsan-si, 38541, Gyeongsangbuk-do, Republic of Korea
[b] Department of Materials Science and Engineering, Pukyong National University, 45, Yongso-ro, Nam-Gu, Busan, 48513, Republic of Korea
[c] Department of Mechanical Engineering (Department of Aeronautics, Mechanical and Electronic Convergence Engineering), Kumoh National Institute of Technology, 61 Daehak-ro, Gumi, 39177, Gyeongbuk, Republic of Korea
[d] Department of Physics, Indian Institute of Technology Hyderabad, Kandi, 502284, Telangana, India
[e] School of Materials Science and Engineering, Kyungpook National University, 80 Daehak-ro, Buk-gu, Daegu, 41566, Republic of Korea
[f] Department of Biofibers and Biomaterials Science, Kyungpook National University, Daegu, 41566, Republic of Korea
[g] Division of Advanced Materials Engineering, Jeonbuk National University, Jeonju, Jeonbuk, Republic of Korea
[h] Department of Electronic Engineering, Yeungnam University, Gyeongsan, 38541, Republic of Korea
[i] Korea Institute of Materials Science (KIMS), 797 Changwondaero, Seongsan-gu, Changwon, 51508, Gyeongnam, Republic of Korea

ARTICLE INFO

Keywords:
Magnetoelectric
Magneto-mechano-electric conversion
Energy harvesting
Photon flash annealing
Self-powered IoT sensor

ABSTRACT

In this paper, we demonstrate a boosted output magneto-mechano-electric (MME) generator consisting of piezoelectric $Pb(Mg_{1/3}Nb_{2/3})O3\text{-}Pb(Zr,Ti)O3$ (PMN-PZT) single crystal and laminated FeBSi alloy (Metglas) prepared by employing photon flash annealing (PFA) treatment. The high-temperature PFA treatment with millisecond-level short pulse irradiation on the Metglas sheet induces surface nanocrystallization, enhances magnetostrictive and mechanical responses. The PFA-treated Metglas-based MME generator exhibits a strong magnetoelectric coupling coefficient of 215 V/cm•Oe, an open-circuit root mean square (RMS) voltage of 26 V, and RMS output power of 3 mW at an AC magnetic field of 8 Oe. These values are noticeably larger (~100 % enhancement for output power) than those of pristine Metglas-based MME generators due to the enhanced piezomagnetic coefficient and mechanical quality factor of PFA Metglas. Finally, the output electric energy of the PFA-treated MME generator is utilized to drive an Internet of Things (IoT) device by integrating the MME generator with a power management circuit, a storage capacitor, and an IoT temperature sensor.

1. Introduction

In the 4th industrial revolution, Internet of Things (IoT) sensors have attracted significant attention for their capacity to collect and analyze data related to the environment, public safety, biomedical healthcare, and industry [1–5]. However, conventional batteries as a power source for numerous IoT sensors have the drawback of limited electric capacity, which requires periodic replacement of depleted batteries with accompanying immense labor and cost [1,6,7]. To address these issues, energy harvesting technology has introduced IoT devices for developing self-powered, maintenance-free, and sustainable IoT applications [6,8,9].

Numerous energy conversion mechanisms have been used in energy harvesting technologies, including piezoelectric [6,10–13], pyroelectric [14], photovoltaic [15,16], triboelectric [17–20], and magneto-mechano-electric (MME) conversion [8,9,21–25]. Among these, the MME generator is a good candidate for self-powered IoT systems to generate electricity from ambient magnetic fields that are

* Corresponding author.
** Corresponding author.
E-mail addresses: jhryu@ynu.ac.kr (J. Ryu), gthwang@pknu.ac.kr (G.-T. Hwang).
[1] These authors contributed equally to this work.

https://doi.org/10.1016/j.mtphys.2025.101758
Received 19 March 2025; Received in revised form 17 May 2025; Accepted 27 May 2025
Available online 28 May 2025
2542-5293/© 2025 The Authors. Published by Elsevier Ltd. This is an open access article under the CC BY-NC license (http://creativecommons.org/licenses/by-nc/4.0/).

generated around electric cables of power transmission lines, building infrastructure, and electronic devices. An MME generator composed of a piezoelectric material, magnetostrictive cantilever, and magnetic proof mass first converts an alternating current (AC) magnetic field into mechanical motion by a magnetostriction effect (magneto-mechanic coupling), which is then converted into electrical energy by a piezoelectric effect (mechano-electric coupling) [31].

To improve the electric output of MME generators, many research results have been reported not only adopting high-performance piezoelectric and magnetostrictive materials but also modifying device geometry and structure. For example, Ryu et al. fabricated MME generators with improved mechanical quality factor (Q_m) and dielectric loss (tanδ) (or minimized electromechanical losses) by doping of hardener Mn in $Pb(Mg_{1/3}Nb_{2/3})O_3$-$Pb(Zr,Ti)O_3$ (PMN-PZT) single crystals [26]. It exhibited an open-circuit voltage of 94 V and a short-circuit current of 120 μA under a gentle magnetic field of 7 Oe. Annapureddy et al. adopted a specially textured Fe-Ga magnetostrictive alloy and (011)-oriented PMN-PZT crystal for a high-performance MME harvester, which generated an output power of 3.8 mW to operate an IoT sensor [24].

In particular, FeBSi alloy (Metglas) foils are widely utilized as a magnetostrictive cantilever structure in MME generators, which has a high piezomagnetic coefficient and an enormous magnetic permeability [27]. Many attempts have also been made to enhance the output performance of MME generators based on multilayer Metglas lamination by design of harvester architecture and optimization of interfacial adhesion layer [25,28–30]. Flash lamps are an alternative photonic annealing source for commercialization due to their ultrafast (μs to ms) interaction, large-scale processability, and outstanding light output efficiency [31]. With high-intensity photon flash annealing (PFA), bulk metal sheets can be abruptly heated to the crystallization temperature by non-radiative relaxation in the form of atomic lattice vibrations and then rapidly cooled to form nano-scale crystals in the microstructures [32]. In this way, the Metglas sheet with an amorphous phase could also be annealed with the flashlight process to induce nano-scale crystallization for further improvement of magneto-mechanical coupling performance in MME energy harvesting.

Herein, we have demonstrated an MME generator consisting of a Metglas laminate and PMN-PZT single crystal fiber composite (SFC) by employing PFA treatment on Metglas sheets to improve the output performance of the MME generator. The instant high-temperature PFA with an ms-level short pulse on the Metglas alloy-derived surface nanocrystallization enhanced the soft magnetic property, piezomagnetic property, and Q_m. After the PFA treatment, the piezomagnetic coefficient and Q_m values of the Metglas laminate were increased by up to 37 % and 131.5 %, respectively, compared to the pristine Metglas laminate. The PFA-treated MME generator displayed a strong magnetoelectric (ME) voltage coefficient (α_{ME}) of 215 V/cm•Oe, an open-circuit root mean square (RMS) voltage of 26 V, and a short-circuit current of 0.46 mA at a resonance condition of 60 Hz. In addition, the PFA MME device generated a maximum RMS output power of 3.0 mW at an AC magnetic field of 8 Oe, which is two times higher than that of a pristine Metglas-based MME generator. Finally, the electric power from the PFA-treated MME generator was utilized directly to operate an environmental IoT sensor system by integrating with a power management circuit, a storage capacitor, and an IoT temperature sensor. With this self-powered system, the IoT sensor can incessantly monitor surrounding temperature and wirelessly transfer the measured information to a monitoring computer without needing a battery or other power source.

2. Materials and methods

2.1. Photon flash annealing for the Metglas foil

The Metglas sheet having a thickness of 25 μm (2605SA1, Hitachi Metal Co.) was cut in the dimensions of 60 (L) × 20 (W) mm^2. Metglas 2605SA1 was selected as the magnetostrictive layer due to its amorphous structure, which offers several advantages for MME applications. Its low magnetic anisotropy and high initial magnetic permeability facilitate strong magnetostrictive response under low-amplitude AC magnetic fields. Additionally, its narrow magnetic hysteresis minimizes energy loss, while the uniform amorphous phase enables controlled surface nanocrystallization through PFA, further enhancing its magnetic softness [33]. The ribbon form and mechanical flexibility of Metglas also make it suitable for multilayer cantilever configurations used in this study. The PMN-PZT SFC was chosen as the piezoelectric counterpart due to its high piezoelectric coefficient, mechanical compliance, and compatibility with laminated multilayer structures operating in bending mode [24]. Key physical properties of both materials are summarized in Tables S1 and S2 (Supporting Information) for reference. The cut Metglas foils were irradiated with two continuous shots of the pulsed flashlights. PFA was performed using a xenon flash lamp system (HI-PULSE 15000, PSTEK Co., Ltd) that emits a broad spectrum of white light, approximately ranging from 300 to 1000 nm. The irradiation condition consisted of two consecutive pulses, each with an input power of 5.1 kW and a pulse duration of 2.0 ms, applied with a time interval of 250 ms.

2.2. Fabrication of MME generator using photon flash annealed Metglas

The (011)-oriented d_{32} mode PMN-PZT SFC (external dimensions: 20 × 13 × 0.15 mm^3, Ceracomp Co. Ltd) was a piezoelectric layer. The PFA Metglas foils were laminated by stacking 10 layers in the Teflon mold. Each layer was bonded using a thermal cure epoxy resin (3M™ Scotch-Weld Epoxy Adhesive DP-460 EG), and then a force of 1 ton was loaded on the mold to densely stack the Metglas lamination as well as to minimize the adhesion layers. The Metglas lamination was heat-treated at 70 °C for 1 h to cure the epoxy resin. The Metglas lamination was bonded with the SFC using the epoxy resin and then clipped with a two-slot zig, followed by curing at 70 °C for 3 h, resulting in the bilayer composite. Two pieces of NdFeB permanent magnets (20× 5 × 2 mm^3) were attached at an optimized position on the composite for a resonance frequency of 60 Hz as a magnetic proof mass to fabricate the MME generator.

2.3. Characterization

The magnetic hysteresis (B-H) loops of the Metglas laminates were obtained using a B-H analyzer (Remagraph C-500, Magnet physic) by applying the magnetic field along the length direction of the Metglas laminate. The magnetic field-dependent magnetostriction of the 10 layers of Metglas laminate was characterized using the strain-gauge method. The piezomagnetic coefficient (q_{11}) along the longitudinal direction of the Metglas laminate was evaluated from the slope of magnetostriction curves.

To verify the resonance tuning of the PFA-treated MME harvester, impedance analysis was conducted using an impedance analyzer (4294A, Agilent). The resulting Z-θ plot (Fig. S1a in the Supporting Information) confirmed a resonance frequency at 60 Hz and an anti-resonance frequency at 63.6 Hz, demonstrating that the magnetic proof mass was appropriately positioned to match the first bending-mode resonance with the commercial AC power frequency. A top-view image of the device mounted on the measurement clamp is provided in Fig. S1b (see the Supporting Information), showing that the magnet was attached 0.8 cm from the free end of the cantilever. This position was determined through iterative tuning to achieve optimal resonance behavior at 60 Hz.

The resonance characteristics of the MME generator, including vibrational amplitude and α_{ME}, were measured under a low AC magnetic field amplitude of 0.1 Oe to precisely determine the resonance frequency while avoiding nonlinear magnetic or mechanical effects. The tip displacements of the MME generator were obtained under the AC magnetic field of 0.1 Oe by laser Doppler vibrometer (LDV, OFV-5000, Polytec). The vibration amplitude was swept according to the frequency through the fast Fourier transform (FFT) method. The Q_m was estimated from the result of the vibration amplitude peak using the -3dB method ($Q_m = f_r/\Delta f$) using the resonance frequency (f_r) and -3 dB bandwidth (Δf) of the vibration amplitude peak. The α_{ME} evaluation for the MME generator was performed as a function of AC magnetic oscillation (H_{ac}) frequency from 45 to 75 Hz at a direct current (DC) magnetic bias field (H_{dc}) of 0 Oe. A H_{ac} of 0.1 Oe was applied in the longitudinal direction to the MME generator located at the center of the Helmholtz coil (M-MHC125, MMS company). The output voltage from MME device was measured by sweeping the Hac driving frequency using a lock-in amplifier (SR-850, Stanford Research Systems). The measured output voltage was divided by the thickness of the SFC (150 μm) and Hac to calculate the value of α_{ME}.

2.4. Output performance of the MME generator

For performance evaluation under practical conditions, the MME generator was subsequently tested at an AC magnetic field amplitude of 8 Oe, which reflects the typical ambient magnetic field strength near commercial AC power lines [34]. This field strength was selected to ensure sufficient mechanical excitation and to assess the energy harvesting capability of the device under realistic operating environments. The AC magnetic field of 8 Oe at 60 Hz was applied to MME generators using a Helmholtz coil to measure the generated output voltage. The voltage waveform signals were monitored using an oscilloscope (WaveSurfer 44Xs-A, Teledyne LeCroy, NY, USA). To determine the maximum output power of the MME generator at the optimal load resistance, the external load resistance was applied by connecting an electronically controlled resistance decade box (OS 260, IET Labs, Inc.) to the measurement circuit parallelly. The V_{rms} was recorded across the various load resistances (R_L) ranging from 1 kΩ to 1 MΩ, and the output power (P_{rms}) was determined using the expression $P_{rms} = V_{rms}^2/R_L$.

3. Results and discussion

Fig. 1a schematically depicts the fabrication process of the MME generator utilizing PFA-treated Metglas laminate. The amorphous Metglas was annealed in the air by a high-intensity light pulse, which causes oxidation at the local surface by inducing temporal thermal energy to enhance the magneto-mechanical properties without structural brittleness (Fig. 1a–i) [35–37]. With an ultra-short flash pulse treatment on the amorphous Metglas, an oxygen-rich region with partial nano-crystals

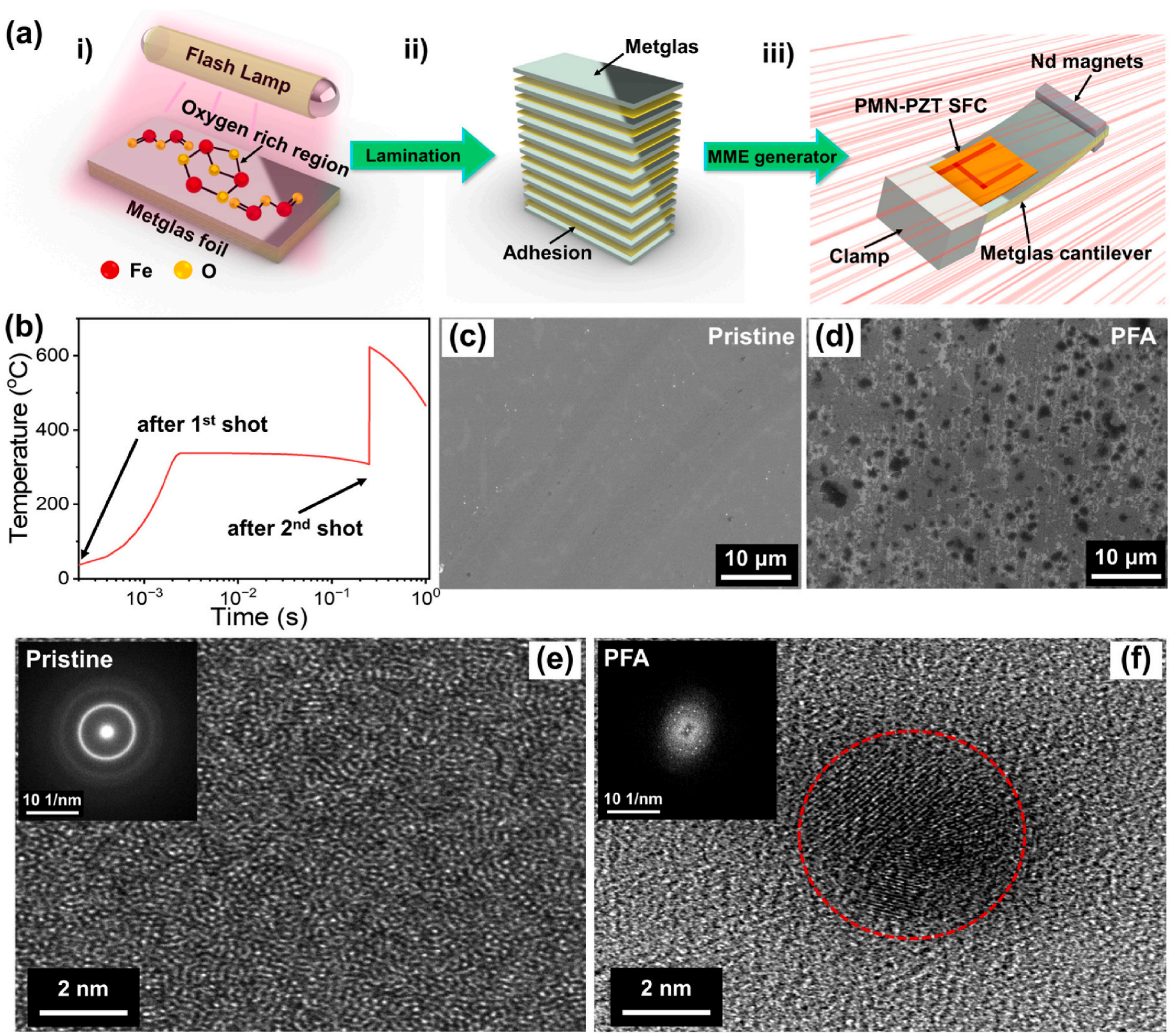

Fig. 1. (a) Schematic representation of the fabrication process for the MME generator. (i) The Xenon PFA induces Metglas nanocrystallization and oxidation. (ii) The Metglas sheets were laminated using an epoxy resin to form a magnetostrictive cantilever. (iii) The cantilever-structured MME generator is composed of a Nd magnet, clamp, and MME composite (Metglas laminate and piezoelectric SFC). (b) Numerically simulated temperature profile of Metglas surface by PFA condition. (c) and (d) SEM images of pristine Metglas and PFA-treated Metglas. (e) and (f) HRTEM images and corresponding FFT patterns (inset) of pristine Metglas and PFA-treated Metglas.

could be successfully formed on the surface of the Metglas [38]. The annealed Metglas sheets were laminated with epoxy resin to form a magnetostrictive cantilever structure (Fig. 1a–ii). The Metglas laminate structure with interfacial adhesion layers is better than a single sheet for MME conversion since the magnetostriction force applied on the piezoelectric part is proportional to the cross-sectional surface area of the multiple Metglas layers [28]. The MME cantilever generator is fabricated by combining a Nd permanent magnet-proof mass with a bilayer composite consisting of Metglas lamination and PMN-PZT SFC, as schematically shown in Fig. 1a–iii. The external magnetic field excitation deforms the magnetostrictive Metglas laminate in the longitudinal direction, which transfers strain to the piezoelectric phase in the MME generator, thus leading to piezopotential generation in the thickness direction by transverse piezoelectric d_{32} mode. The tip mass magnets on the MME generator helped to promote periodic up-and-down bending vibrations (magnetic torque) of the cantilever by creating mutual interactions with the surrounding AC magnetic field.

A theoretical simulation was performed to estimate time-dependent temperature alternation of the Metglas surface under PFA using COMSOL Multiphysics. The simulated flash condition was composed of two consecutive flash illuminations (5.1 kW and pulse duration of 2 ms) with a time interval of 250 ms. Fig. 1b shows the calculated temperature profile of the Metglas surfaces under a flashlight condition. It is widely known that multiple flashlight irradiations can generate a significant temperature increment at the surface of a target material via repeated thermal accumulation [31]. The peak surface temperature of the Metglas sheets during PFA was theoretically estimated to be approximately 623 °C using COMSOL Multiphysics simulation, as direct experimental measurement was challenging due to the extremely short flash duration. This transient thermal input exceeds the crystallization temperature of Metglas (~560 °C), enabling localized surface nanocrystallization while preserving the amorphous nature of the bulk [38]. Further, we performed scanning electron microscope (SEM) and high-resolution transmission electron microscopy (HRTEM) measurements to examine the effect of PFA on the microstructural properties of Metglas. Fig. 1c and d displays a SEM image of the pristine Metglas and PFA-treated Metglas surface. After the PFA process, short-range microstructural change was observed with the presence of oxygen-rich dark color regions on the Metglas surface from an energy dispersive spectrometer (EDS) analysis (Fig. S2 in the Supporting Information), providing evidence of partial surface oxidation of Metglas during the PFA treatment. Fig. 1e and f shows HRTEM images and their corresponding FFT patterns (insets) of the pristine and PFA-treated Metglas sheets, respectively. The FFT pattern of pristine Metglas (Fig. 1e) exhibits a uniform diffuse ring, which is a typical signature of an amorphous structure lacking long-range atomic order. Consistently, the corresponding HRTEM image shows no lattice fringes or crystalline domains. In contrast, the PFA-treated Metglas (Fig. 1f) displays localized lattice fringes in the HRTEM image (highlighted by a red circle), along with discrete bright diffraction spots in the FFT pattern. These morphological changes are attributed to partial surface nanocrystallization induced by the PFA process. The high-intensity photon pulse transiently heats the surface, increasing atomic mobility in localized regions and enabling nucleation of nanocrystalline domains, while the surrounding matrix remains amorphous [39]. As a result, the fully amorphous pristine sample shows a ring-like FFT pattern, whereas the PFA-treated sample exhibits a dot-like morphology due to the formation of discrete crystalline regions. This indicates that PFA enables localized structural transformation without compromising the overall amorphous nature of Metglas. The estimated size of the nanocrystal was approximately 5 nm, based on the HRTEM image analysis. Although the crystallinity was not quantitatively evaluated using additional characterization techniques, the emergence of nanocrystalline features in the FFT pattern, combined with the enhanced magnetostrictive response and mechanical quality factor, provides strong indirect evidence of localized nanocrystal formation.

The magnetic field intensity can be controlled by varying the input AC current into the Helmholtz coil. Note that a high α_{ME} is essential for the high output performance of MME generators. The α_{ME} is a result of the mechanical interaction between the magnetostrictive and piezoelectric layers, which is explained by the following equation [21,40].

$$\alpha_{ME} = \frac{\Delta E}{\Delta H} = \frac{\Delta E}{\Delta S} \times \frac{\Delta S}{\Delta B} \times \frac{\Delta B}{\Delta H} \quad (1)$$

where E is the electric field induced from the piezoelectric phase, S is the strain caused by magnetostriction, B is the magnetic flux density within the magnetostrictive phase, and H is the externally applied AC magnetic field. Equation (1) indicates that α_{ME} can be enlarged by enhancing $\Delta B/\Delta H$, which is termed as the magnetic permeability and piezomagnetic properties ($\Delta S/\Delta B$) of the magnetostrictive phase. Fig. 2a shows the B-H hysteresis loops of pristine and PFA Metglas laminates. The PFA-treated Metglas sheets showed significantly improved soft magnetic properties and reduced hysteresis. The value of the maximum magnetic permeability ($\mu_{\max}$) is calculated from the $\Delta B/\Delta H$ slope. The PFA Metglas laminate has a $\mu_{\max}$ of 9960 H/m, while the pristine Metglas laminate has a value of 9080 H/m. The PFA-treated Metglas laminate also showed a similar response to that of the pristine Metglas but with enhanced soft magnetic properties, which is attributed to the surface nanocrystallization-induced residual stress relaxation and reduced local density fluctuations [41]. Fig. 2b shows the experimental setup utilized to measure the output performance of the MME generator at external magnetic fields produced by a Helmholtz coil. The MME cantilever structure was rigidly clamped by a Bakelite jig, and a non-magnetic metal holder was placed in the center of the Helmholtz coil to apply a uniform AC magnetic field (right side of Fig. 2b). The MME generator in this study was designed as a cantilever structure operating in its 1st bending resonance mode. To optimize the MME output performance, the cantilever geometry was engineered by considering the trade-off between mechanical flexibility and stress transfer to the piezoelectric layer [42]. A thinner cantilever allows larger vibration amplitudes but results in lower stress applied to the piezoelectric element, while a thicker cantilever increases stress delivery at the expense of reduced displacement. Based on this design principle, a laminated structure composed of ten 25 μm-thick Metglas foils was adopted as the magnetostrictive cantilever. The total thickness of the laminate, including the adhesive layers between Metglas sheets, was approximately 280 μm, implying an average adhesive thickness of 3~4 μm per interlayer [28]. This configuration provides a well-balanced mechanical response, enabling efficient vibration-driven deformation of the piezoelectric layer and enhanced energy harvesting performance. The MME structure was fabricated based on the assumption that each Metglas layer exhibits comparable piezomagnetic properties, as all ten foils were processed under identical PFA conditions prior to lamination. While measuring the piezomagnetic coefficient of each layer individually would be ideal for evaluating potential variation, such measurements require attaching and subsequently removing strain gauges. This removal process can damage the ultrathin Metglas surface or leave adhesive residue, which would impair interfacial bonding and degrade the mechanical integrity of the final laminate. As a result, individual layer characterization was not performed, and the MME structure was designed to function based on the average behavior of the laminated Metglas stack without requiring layer-specific tuning. This approach is supported by the uniform processing conditions and material homogeneity, and ensures both structural reliability and consistent piezomagnetic performance.

The magnetostriction of the pristine and PFA-treated Metglas laminates was compared by measuring the surface strain in the longitudinal direction by sweeping H_{dc} from −80 Oe to 80 Oe, as shown in Fig. 2c. The measured saturated magnetostriction (λ_s) of the Metglas laminate with PFA was 41.7 ppm, which is almost 63 % larger as compared to the pristine Metglas laminate (25.6 ppm). The piezomagnetic coefficient curves, estimated from the slope of the magnetostriction curves, are displayed in Fig. 2d. Here, the 'slope' refers to the first-order derivative

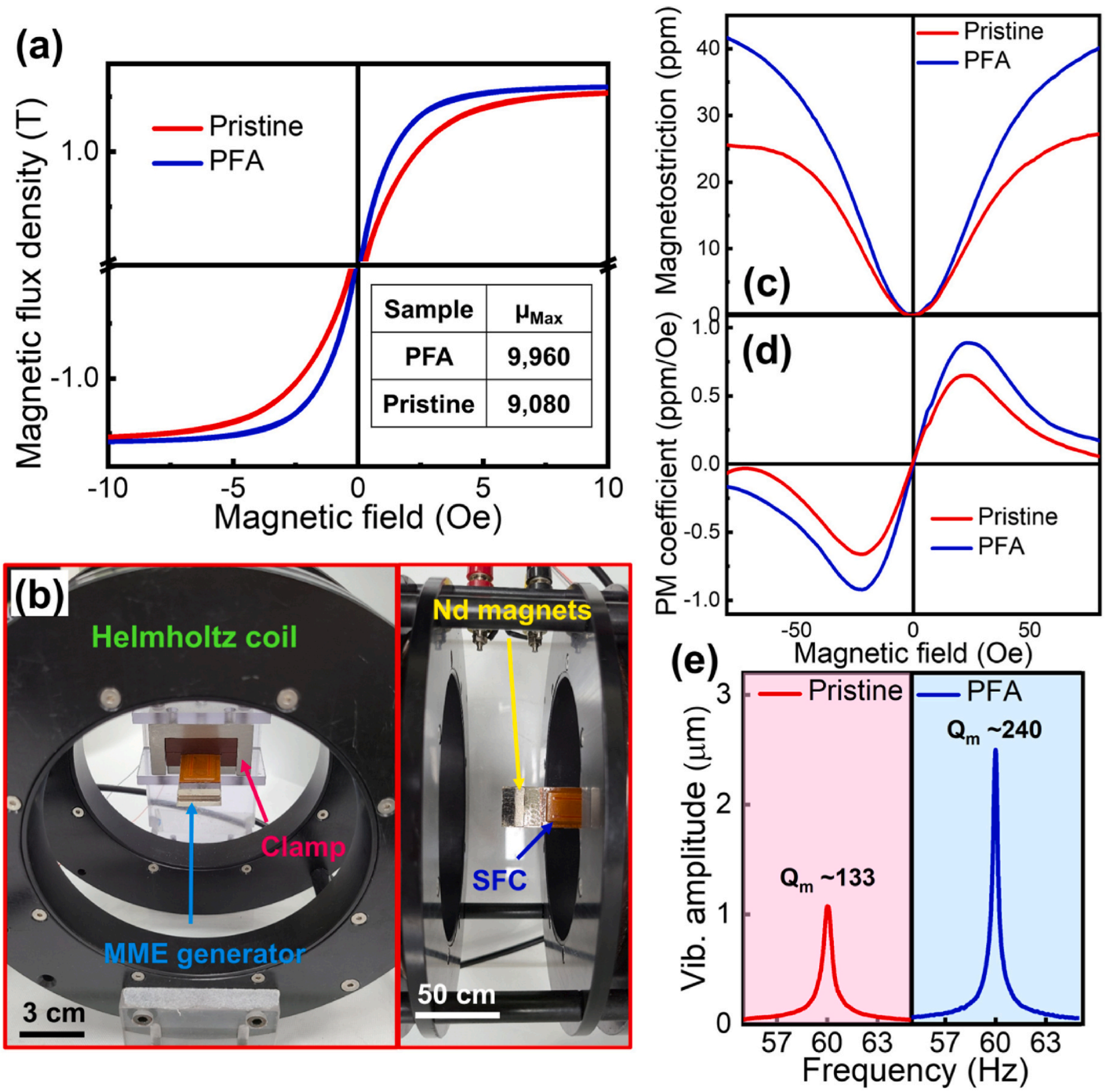

Fig. 2. (a) B-H hysteresis of normal and PFA Metglas sheets. (b) Experimental setup to measure the electric output performance of the MME generator inside the Helmholtz coil. DC magnetic field dependent (c) magnetostriction and (d) piezomagnetic coefficient curves of pristine Metglas and PFA Metglas laminate. (e) The vibration amplitudes of pristine and PFA Metglas laminates were measured by sweeping the frequency in the proximity of the resonance condition (~60 Hz).

($d\lambda/dH$), representing the sensitivity of magnetostriction to the applied magnetic field [43]. Although adhesive layers of pristine Metglas lamination may potentially dampen interlayer strain transfer, the measured saturation magnetostriction (25.6 ppm) was very close to the manufacturer-reported value for single-layer Metglas (27 ppm), indicating that the influence of the adhesive on the magnetostrictive performance was nearly negligible. The PFA Metglas laminate shows enhanced maximum piezomagnetic coefficients of 0.89 ppm/Oe, while the pristine Metglas laminate has a maximum value of 0.65 ppm/Oe. This corresponds to a ~37 % enhancement and indicates that the maximum piezomagnetic coefficient in this study was successfully achieved through the applied PFA treatment. Such improvement is attributed to the partial surface nanocrystallization induced by PFA, which enhances both the magnetostrictive response and the Q_m of the Metglas laminate. This piezomagnetic property enhancement due to the PFA treatment can significantly affect the α_{ME} as it depends on the magnetic field-induced vibration displacement and Q_m [26,39,44,45].

Fig. 2e displays the vibration amplitude of the Metglas laminate measured in the proximity of the resonance frequency (60 Hz) at 0.1 Oe, using a laser Doppler vibrometer (LDV). The Q_m values of the Metglas laminate were obtained using the −3 dB method from the frequency-dependent vibration amplitude curves. The estimated Q_m value of the PFA-treated Metglas laminate was 240, which is ~81 % larger than that of pristine Metglas laminate (Q_m of 133). Similarly, the oscillation displacement of the PFA Metglas laminate was enhanced by 131.5 % with the PFA relative to the pristine Metglas laminate. From this result, it is expected that the magneto-mechanical response of the MME generator incorporating the PFA Metglas could be significantly enhanced with the improved Q_m and oscillation displacement, leading to excellent output performance of the MME generator.

The frequency-dependent α_{ME} of the MME generator in the resonance regime was measured under a H_{ac} of 0.1 Oe, and the zero external H_{dc}, and the results are depicted in Fig. 3a. In the proposed MME generator, a magnetic proof mass was attached to the free end of the cantilever to enable efficient mechanical excitation under an AC magnetic field. The interaction between the alternating field and the magnetic mass produces a dynamic magnetic force, which drives substantial bending-mode vibration of the cantilever even in the absence of an external DC

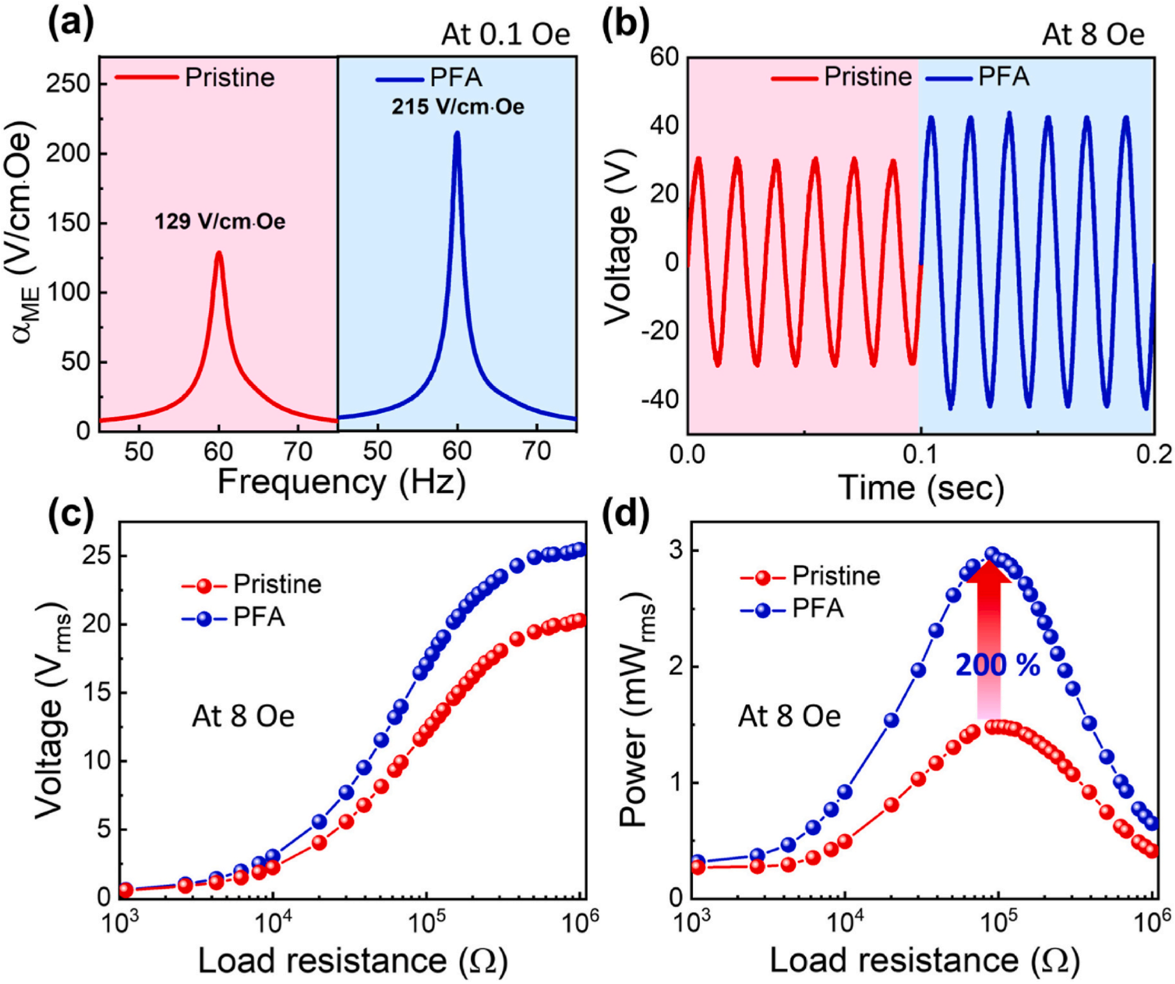

Fig. 3. (a) Resonance ME coupling characteristics and (b) open-circuit voltage waveforms of the MME generators, (c) RMS output voltage, and (d) RMS output power of MME generators of pristine Metglas and PFA Metglas laminate measured as a function of external load resistances.

magnetic bias [46]. While no external H_{dc} was applied, the presence of the permanent magnet at the cantilever tip likely introduces a small local magnetic field to the Metglas laminate, effectively acting as a built-in bias. This local self-bias may contribute to partial domain alignment and facilitate magnetoelectric coupling under zero externally applied DC conditions. This design allows the device to operate effectively under zero DC bias, which is critical for practical energy harvesting near commercial 60 Hz power lines. Moreover, the PFA treatment of the Metglas layer resulted in an increase in initial magnetic permeability (μ_{max} of 9960 H/m), indicating enhanced magnetic softness. This improvement enables the material to respond more sensitively to low-amplitude AC magnetic fields, thereby further supporting ME coupling without relying on external biasing. The MME composite with PFA Metglas laminate exhibited a larger α_{ME} value of 215 V/cm•Oe compared with pristine Metglas composite (129 V/cm•Oe) at their resonance frequency of 60 Hz. This result validates that ME coupling was enhanced significantly due to the improvement of the piezomagnetic property and the vibration displacement amplified by the higher Q_m of the PFA Metglas laminate.

Further, the energy generation performance of the MME generators with pristine and PFA Metglas laminates was investigated and compared to confirm the enhanced ME coupling derived from the PFA effect. In this regard, the resonance frequency of the MME generators was tuned to 60 Hz by adjusting the position of the magnetic proof mass and applying a H_{ac} of 8 Oe using the Helmholtz coil. The generated open-circuit voltage waveforms of the MME generators are displayed in Fig. 3b. The peak-to-peak voltages (V_{pp}) of the MME generators with PFA Metglas laminate was 88 V, whereas the MME generator with pristine Metglas laminate generated only 61 V. The corresponding short-circuit currents were 0.38 mA and 0.46 mA for the MME generators with pristine and PFA Metglas laminates, respectively, as shown in Fig. S3. To evaluate the performance of MME device under varying AC magnetic field conditions, the output voltage of the PFA-treated MME generator was measured at field amplitudes of 1, 2, 4, 6, and 8 Oe under open-circuit conditions as shown in Fig. S4 (see the Supporting Information). The corresponding peak-to-peak voltages were 6.9 V, 13.4 V, 29.2 V, 72.2 V, and 88 V, respectively, indicating a strong positive correlation between magnetic field strength and voltage response. Based on these results, 8 Oe was selected as a representative field strength, as it aligns with the typical magnetic field range (up to 10 Oe) found near commercial AC power lines [9]. This approach reflects realistic operating conditions and validates the potential of the device for ambient magnetic energy harvesting applications.

The RMS output voltages (V_{rms}) of the MME generators were obtained as a function of external load resistances (R_L), ranging from 1 kΩ to 1 MΩ, as presented in Fig. 3c. The V_{rms} also has shown a similar trend as V_{PP} with a maximum open-circuit V_{rms} of 25.5 V for the FPA Metglas laminate-based MME generator. Further, the corresponding RMS output power (P_{rms}) of MME generators was calculated from the obtained V_{rms} and external R_L using the equation $P_{rms} = V_{rms}^2/R_L$ and displayed in Fig. 3d. The calculated maximum P_{rms} values of the MME generators with pristine and PFA Metglas were 1.5 and 3.0 mW at the optimal R_L

values of 100 and 90 kΩ, respectively. The MME generators with PFA Metglas laminate produced approximately 100 % enhanced output powers than that of pristine Metglas-based MME generator. It is clear that the improvement of the output performance is attributed to the large magneto-mechanical response, which is reasonably demonstrated by the enhanced piezomagnetic and mechanical properties of Metglas sheets after PFA treatment.

The frequency-dependent output characteristics of the PFA-treated MME harvester were further investigated to compare its performance at resonance (60 Hz) and anti-resonance (63.6 Hz) conditions. Under an 8 Oe AC magnetic field, the RMS output voltage reached 25.5 V across a ~1 MΩ load at 60 Hz, while it decreased to 13.2 V at 63.6 Hz. Correspondingly, the RMS output power peaked at 3.0 mW across a 90 kΩ load at resonance, but dropped to 0.37 mW at anti-resonance with a 220 kΩ load. These findings are consistent with the expected behavior of piezoelectric electromechanical systems, in which the minimized mechanical impedance at resonance leads to enhanced vibration amplitude and energy conversion, whereas at anti-resonance, the system exhibits high impedance with suppressed motion [47]. To further support this interpretation, side-view photographs of the MME harvester during operation were captured at both resonance and anti-resonance frequencies. The images clearly show that the vibration displacement of the cantilever is significantly larger at 60 Hz and visibly reduced at 63.6 Hz. These results visually confirm the mechanical resonance behavior and have been included in the Supporting Information (Fig. S5).

Finally, the energy generated from the PFA-treated Metglas laminate-based MME generator was utilized to demonstrate practical applications such as illuminating the light-emitting diodes (LEDs) and constructing a self-powered IoT sensor system. In this regard, a Helmholtz coil for generating a magnetic field of 8 Oe, a conventional full-wave bridge rectifier for converting AC signals into DC signals, and a storage capacitor for storing the rectified energy were used. As shown in Fig. 4a, the rectified electrical energy from the PFA MME generator at 8 Oe was sufficient to illuminate the 100 LEDs continuously under indoor conditions. Further, a self-powered IoT environmental monitoring system was demonstrated to develop an MME generator as a power source in a real-life application, as shown in Fig. 4b–i and 4b-ii. Initially, the output of the MME generator was rectified and then used for charging a 1 mF capacitor to operate the IoT-based temperature sensor (eZ430-RF2500, Texas Instrument). The environmental IoT sensor system senses and transfers the ambient environmental information to the monitoring computer every 10 s through wireless transmission and provides real-time monitoring on the computer screen, as shown in Fig. 4b–iii. Fig. 4c depicts the charging and discharging profile of the 1 mF storage capacitor during the IoT sensor operation by using the output energy of PFA MME generator at 8 Oe. Interestingly, the capacitor was fully charged to 3.5 V within 14 s, and a slight dip in the voltage (~3.2 V) was observed while connecting the sensor but quickly restored to the initial value of 3.5 V. However, no significant change in the capacitor voltage was noticed while sensing and transmitting the ambient environmental data to the monitoring system, thanks to the larger and continuous energy generation by the PFA MME generator. The results show that the MME composite generator with high energy generation performance enabled by the PFA process has the potential to be a sustainable energy source for realizing self-powered environment monitoring systems.

4. Conclusions

In summary, we demonstrated an MME generator composed of piezoelectric PMN-PZT crystal and PFA-treated magnetostrictive Metglas alloy with improved magnetic and mechanical properties. The enhanced piezomagnetic and mechanical properties of PFA-treated Metglas enable a promising approach to fabricate a high-performance MME generator. The PFA-treated MME generator exhibited an improved α_{ME} and maximum RMS output power as compared to that of a pristine Metglas-based MME generator. The PFA MME generator could

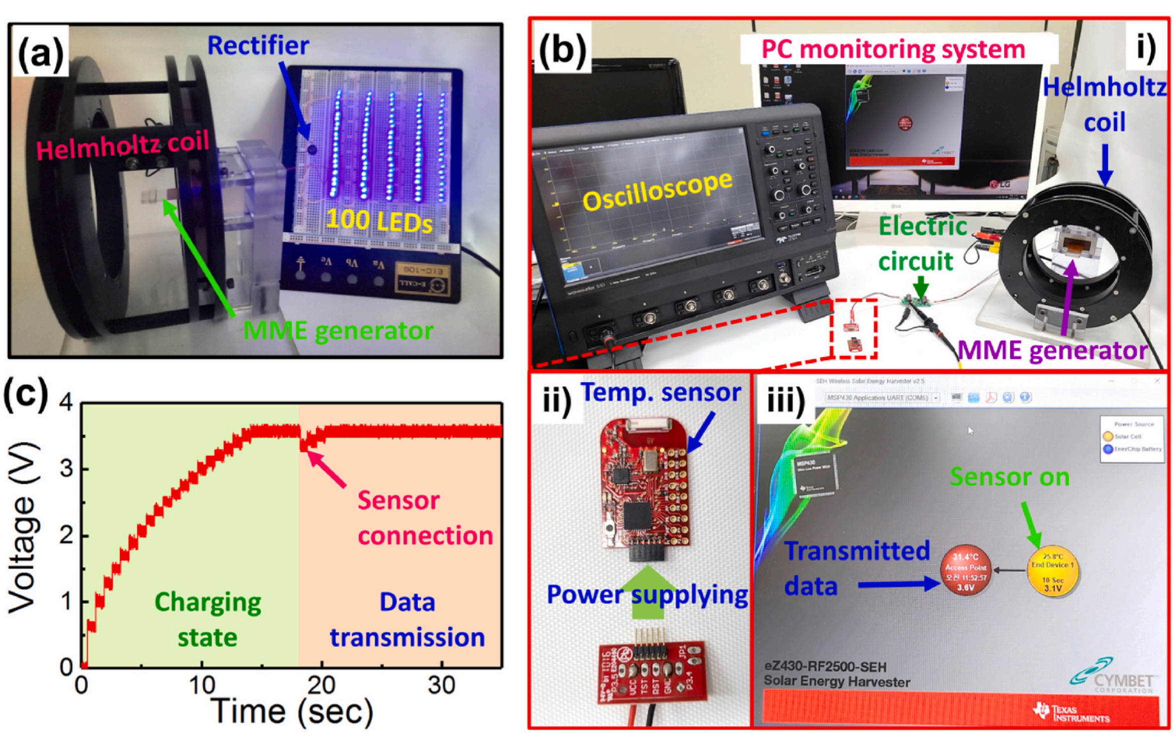

Fig. 4. (a) The generated electric energy from the MME generator with the PFA Metglas laminate enabled 100 LEDs to be turned on. (b) Demonstration of a self-powered IoT environment monitoring system. (i) Photograph of the temperature monitoring system consisting of an MME generator, energy conversion circuit, digital oscilloscope, Helmholtz coil, PC monitoring, and IoT temperature sensor. (ii) The generated power from the MME generator is supplied to the IoT sensor. (iii) The measured ambient temperature data from the sensor is transmitted to the PC monitor screen in real time. (c) The charging and discharging voltage response of the storage capacitor while sensor operation by the MME generator.

be able to generate an open-circuit V_{rms} of 26 V, a short-circuit current of 0.46 mA, and a maximum P_{rms} of 3.0 mW under a magnetic field of 8 Oe, which are significantly higher than the values of a pristine Metglas laminate-based MME generator. The generated electrical energy from the PFA MME harvesting device could continuously operate an IoT environmental sensor without any significant voltage drop in the storage capacitor. These findings demonstrate the practical feasibility of a PFA-treated MME generator as a sustainable energy source in self-powered IoT devices.

CRediT authorship contribution statement

Hyunseok Song: Writing – original draft, Visualization, Validation, Formal analysis, Data curation. **Srinivas Pattipaka:** Writing – original draft, Validation, Formal analysis, Data curation. **Yun Sik Hwang:** Visualization, Software. **Mahesh Peddigari:** Validation, Investigation. **Yuho Min:** Writing – review & editing, Investigation. **Kyeongwoon Chung:** Methodology, Investigation. **Jung Hwan Park:** Visualization, Software. **Chang Kyu Jeong:** Investigation, Conceptualization. **Han Eol Lee:** Visualization, Validation. **Jongmoon Jang:** Methodology, Investigation. **Kwi-Il Park:** Resources, Conceptualization. **Sung-Dae Kim:** Resources, Methodology, Investigation. **Jaewon Jeong:** Resources, Methodology, Funding acquisition. **Woon-Ha Yoon:** Resources, Conceptualization. **Jungho Ryu:** Writing – review & editing, Supervision, Resources, Project administration, Methodology, Funding acquisition, Conceptualization. **Geon-Tae Hwang:** Writing – review & editing, Writing – original draft, Validation, Supervision, Resources, Project administration, Funding acquisition, Conceptualization.

Declaration of competing interest

The authors declare the following financial interests/personal relationships which may be considered as potential competing interests: Geon-Tae Hwang reports financial support was provided by National Research Foundation of Korea. Jungho Ryu reports financial support was provided by National Research Foundation of Korea. Jungho Ryu reports financial support was provided by Korea Institute for Advancement of Technology. Jaewon Jeong reports financial support was provided by National Research Foundation of Korea. If there are other authors, they declare that they have no known competing financial interests or personal relationships that could have appeared to influence the work reported in this paper.

Acknowledgements

The work at PKNU was supported by the National Research Foundation of Korea (RS-2025-00513047) grant funded by the Ministry of Science and ICT (MSIT). The work conducted at YU was supported by the National Research Foundation of Korea (NRF) grant funded by the Korean government (MSIT) (No. 2023R1A2C2005864) and 'Industrial innovation talent growth support project' of the Korean Ministry of Trade, Industry and Energy (MOTIE), operated by Korea Institute for Advancement of Technology (KIAT) (No. P0023676, Expert Training Project for the eco-friendly metal material industry). The work at KIMS was supported by the Nano & Material Technology Development Program through the National Research Foundation of Korea (NRF) funded by Ministry of Science and ICT (RS-2023-00282305).

Appendix A. Supplementary data

Supplementary data to this article can be found online at https://doi.org/10.1016/j.mtphys.2025.101758.

Data availability

Data will be made available on request.

References

[1] J. Gubbi, R. Buyya, S. Marusic, M. Palaniswami, Internet of Things (IoT): a vision, architectural elements, and future directions, Future Gener. Comput. Syst. 29 (2013) 1645–1660, https://doi.org/10.1016/j.future.2013.01.010.

[2] L. Atzori, A. Iera, G. Morabito, The Internet of Things: a survey, Comput. Netw. 54 (2010) 2787–2805, https://doi.org/10.1016/j.comnet.2010.05.010.

[3] J.M. Perkel, The Internet of Things comes to the lab, Nature 542 (2017) 125–126, https://doi.org/10.1038/542125a.

[4] H.W. Choi, D.-W. Shin, J. Yang, S. Lee, C. Figueiredo, S. Sinopoli, K. Ullrich, P. Jovančić, A. Marrani, R. Momentè, J. Gomes, R. Branquinho, U. Emanuele, H. Lee, S.Y. Bang, S.-M. Jung, S.D. Han, S. Zhan, W. Harden-Chaters, Y.-H. Suh, X.-B. Fan, T.H. Lee, M. Chowdhury, Y. Choi, S. Nicotera, A. Torchia, F.M. Moncunill, V.G. Candel, N. Durães, K. Chang, S. Cho, C.-H. Kim, M. Lucassen, A. Nejim, D. Jiménez, M. Springer, Y.-W. Lee, S. Cha, J.I. Sohn, R. Igreja, K. Song, P. Barquinha, R. Martins, G.A.J. Amaratunga, L.G. Occhipinti, M. Chhowalla, J. M. Kim, Smart textile lighting/display system with multifunctional fibre devices for large scale smart home and IoT applications, Nat. Commun. 13 (2022) 814, https://doi.org/10.1038/s41467-022-28459-6.

[5] C. Polyzoidis, K. Rogdakis, E. Kymakis, Indoor perovskite photovoltaics for the Internet of things—challenges and opportunities toward market uptake, Adv. Energy Mater. 11 (2021): 2101854, https://doi.org/10.1002/aenm.202101854.

[6] G.-T. Hwang, V. Annapureddy, J.H. Han, D.J. Joe, C. Baek, D.Y. Park, D.H. Kim, J. H. Park, C.K. Jeong, K.-I. Park, J.-J. Choi, D.K. Kim, J. Ryu, K.J. Lee, Self-powered wireless sensor node enabled by an aerosol-deposited PZT flexible energy harvester, Adv. Energy Mater. 6 (2016): 1600237, https://doi.org/10.1002/aenm.201600237.

[7] Z.L. Wang, J. Chen, L. Lin, Progress in triboelectric nanogenerators as a new energy technology and self-powered sensors, Energy Environ. Sci. 8 (2015) 2250–2282, https://doi.org/10.1039/C5EE01532D.

[8] H. Lee, R. Sriramdas, P. Kumar, M. Sanghadasa, M.G. Kang, S. Priya, Maximizing power generation from ambient stray magnetic fields around smart infrastructures enabling self-powered wireless devices, Energy Environ. Sci. 13 (2020) 1462–1472, https://doi.org/10.1039/C9EE03902C.

[9] J. Ryu, J.-E. Kang, Y. Zhou, S.-Y. Choi, W.-H. Yoon, D.-S. Park, J.-J. Choi, B.-D. Hahn, C.-W. Ahn, J.-W. Kim, Y.-D. Kim, S. Priya, S.Y. Lee, S. Jeong, D.-Y. Jeong, Ubiquitous magneto-mechano-electric generator, Energy Environ. Sci. 8 (2015) 2402–2408, https://doi.org/10.1039/C5EE00414D.

[10] S. Priya, H.-C. Song, Y. Zhou, R. Varghese, A. Chopra, S.-G. Kim, I. Kanno, L. Wu, D. S. Ha, J. Ryu, R.G. Polcawich, A review on piezoelectric energy harvesting: materials, methods, and circuits, Energy Harvest. Syst. 4 (2019) 3–39, https://doi.org/10.1515/ehs-2016-0028.

[11] N. Sezer, M. Koç, A comprehensive review on the state-of-the-art of piezoelectric energy harvesting, Nano Energy 80 (2021): 105567, https://doi.org/10.1016/j.nanoen.2020.105567.

[12] X. Liu, Y. Shang, J. Zhang, C. Zhang, Ionic liquid-assisted 3D printing of self-polarized β-PVDF for flexible piezoelectric energy harvesting, ACS Appl. Mater. Interfaces 13 (2021) 14334–14341, https://doi.org/10.1021/acsami.1c03226.

[13] G.-T. Hwang, Y. Kim, J.-H. Lee, S. Oh, C.K. Jeong, D.Y. Park, J. Ryu, H. Kwon, S.-G. Lee, B. Joung, D. Kim, K.J. Lee, Self-powered deep brain stimulation via a flexible PIMNT energy harvester, Energy Environ. Sci. 8 (2015) 2677–2684, https://doi.org/10.1039/C5EE01593F.

[14] R.A. Surmenev, R.v. Chernozem, I.O. Pariy, M.A. Surmeneva, A review on piezo- and pyroelectric responses of flexible nano- and micropatterned polymer surfaces for biomedical sensing and energy harvesting applications, Nano Energy 79 (2021): 105442, https://doi.org/10.1016/j.nanoen.2020.105442.

[15] M. de Cea, A.H. Atabaki, R.J. Ram, Energy harvesting optical modulators with sub-attojoule per bit electrical energy consumption, Nat. Commun. 12 (2021) 2326, https://doi.org/10.1038/s41467-021-22460-1.

[16] J. Zhao, R. Ghannam, K.O. Htet, Y. Liu, M. Law, V.A.L. Roy, B. Michel, M.A. Imran, H. Heidari, Self-powered implantable medical devices: photovoltaic energy harvesting review, Adv. Healthcare Mater. 9 (2020): 2000779, https://doi.org/10.1002/adhm.202000779.

[17] M.S. Kwak, K.-W. Lim, H.Y. Lee, M. Peddigari, J. Jang, C.K. Jeong, J. Ryu, W.-H. Yoon, S.N. Yi, G.-T. Hwang, Multiscale surface modified magneto-mechano-triboelectric nanogenerator enabled by eco-friendly NaCl imprinting stamp for self-powered IoT applications, Nanoscale 13 (2021) 8418–8424, https://doi.org/10.1039/D1NR01336J.

[18] C. Wu, A.C. Wang, W. Ding, H. Guo, Z.L. Wang, Triboelectric nanogenerator: a foundation of the energy for the new era, Adv. Energy Mater. 9 (2019): 1802906, https://doi.org/10.1002/aenm.201802906.

[19] Z.L. Wang, Triboelectric nanogenerator (TENG)—sparking an energy and sensor revolution, Adv. Energy Mater. 10 (2020): 2000137, https://doi.org/10.1002/aenm.202000137.

[20] W. Liu, Z. Wang, G. Wang, G. Liu, J. Chen, X. Pu, Y. Xi, X. Wang, H. Guo, C. Hu, Z. L. Wang, Integrated charge excitation triboelectric nanogenerator, Nat. Commun. 10 (2019) 1426, https://doi.org/10.1038/s41467-019-09464-8.

[21] H. Song, D.R. Patil, W.-H. Yoon, K.-H. Kim, C. Choi, J.-H. Kim, G.-T. Hwang, D.-Y. Jeong, J. Ryu, Significant power enhancement of magneto-mechano-electric generators by magnetic flux concentration, Energy Environ. Sci. 13 (2020) 4238–4248, https://doi.org/10.1039/D0EE01574A.

[22] R. Sriramdas, M. Kang, M. Meng, M. Kiani, J. Ryu, M. Sanghadasa, S. Priya, Large power amplification in magneto-mechano-electric harvesters through distributed forcing, Adv. Energy Mater. 10 (2020): 1903689, https://doi.org/10.1002/aenm.201903689.

[23] K.-W. Lim, M. Peddigari, C.H. Park, H.Y. Lee, Y. Min, J.-W. Kim, C.-W. Ahn, J.-J. Choi, B.-D. Hahn, J.-H. Choi, D.-S. Park, J.-K. Hong, J.-T. Yeom, W.-H. Yoon, J. Ryu, S.N. Yi, G.-T. Hwang, A high output magneto-mechano-triboelectric generator enabled by accelerated water-soluble nano-bullets for powering a wireless indoor positioning system, Energy Environ. Sci. 12 (2019) 666–674, https://doi.org/10.1039/C8EE03008A.

[24] V. Annapureddy, S.-M. Na, G.-T. Hwang, M.G. Kang, R. Sriramdas, H. Palneedi, W.-H. Yoon, B.-D. Hahn, J.-W. Kim, C.-W. Ahn, D.-S. Park, J.-J. Choi, D.-Y. Jeong, A. B. Flatau, M. Peddigari, S. Priya, K.-H. Kim, J. Ryu, Exceeding milli-watt powering magneto-mechano-electric generator for standalone-powered electronics, Energy Environ. Sci. 11 (2018) 818–829, https://doi.org/10.1039/C7EE03429F.

[25] Z. Chu, Z. Sun, B. Wang, K. Song, J. Wang, J. Gao, S. Dong, Significantly enhanced power generation from extremely low-intensity magnetic field via a clamped-clamped magneto-mechano-electric generator, Adv. Energy Mater. 12 (2022): 2103345, https://doi.org/10.1002/aenm.202103345.

[26] V. Annapureddy, M. Kim, H. Palneedi, H. Lee, S. Choi, W. Yoon, D. Park, J. Choi, B. Hahn, C. Ahn, J. Kim, D. Jeong, J. Ryu, Low-loss piezoelectric single-crystal fibers for enhanced magnetic energy harvesting with magnetoelectric composite, Adv. Energy Mater. 6 (2016): 1601244, https://doi.org/10.1002/aenm.201601244.

[27] J. Zhai, S. Dong, Z. Xing, J. Li, D. Viehland, Giant magnetoelectric effect in Metglas/polyvinylidene-fluoride laminates, Appl. Phys. Lett. 89 (2006), https://doi.org/10.1063/1.2337996.

[28] G.-T. Hwang, H. Palneedi, B.M. Jung, S.J. Kwon, M. Peddigari, Y. Min, J.-W. Kim, C.-W. Ahn, J.-J. Choi, B.-D. Hahn, J.-H. Choi, W.-H. Yoon, D.-S. Park, S.-B. Lee, Y. Choe, K.-H. Kim, J. Ryu, Enhancement of magnetoelectric conversion achieved by optimization of interfacial adhesion layer in laminate composites, ACS Appl. Mater. Interfaces 10 (2018) 32323–32330, https://doi.org/10.1021/acsami.8b09848.

[29] Z. Yu, H. Qiu, Z. Chu, Z. Sun, M.J. Pourhosseini Asl, F. Li, S. Dong, Significant output power enhancement in symmetric dual-mode magneto-mechano-electric coupled resonators, Adv. Energy Mater. 12 (2022), https://doi.org/10.1002/aenm.202202306.

[30] M.G. Kang, R. Sriramdas, H. Lee, J. Chun, D. Maurya, G.T. Hwang, J. Ryu, S. Priya, High power magnetic field energy harvesting through amplified magneto-mechanical vibration, Adv. Energy Mater. 8 (2018), https://doi.org/10.1002/aenm.201703313.

[31] J.H. Park, G. Hwang, S. Kim, J. Seo, H. Park, K. Yu, T. Kim, K.J. Lee, Flash-induced self-limited plasmonic welding of silver nanowire network for transparent flexible energy harvester, Adv. Mater. 29 (2017), https://doi.org/10.1002/adma.201603473.

[32] E. Yarali, C. Koutsiaki, H. Faber, K. Tetzner, E. Yengel, P. Patsalas, N. Kalfagiannis, D.C. Koutsogeorgis, T.D. Anthopoulos, Recent progress in photonic processing of metal-oxide transistors, Adv. Funct. Mater. 30 (2020), https://doi.org/10.1002/adfm.201906022.

[33] Y. Liu, B. Ducharne, G. Sebald, K. Makihara, M. Lallart, Investigation of energy harvesting capabilities of Metglas 2605SA1, Appl. Sci. 13 (2023), https://doi.org/10.3390/app13063477.

[34] S. Pattipaka, T.W. Park, Y.M. Bae, Y. Na, K. Chung, K. Il Park, J. Ryu, W.I. Park, G. T. Hwang, A nanoscale surface engineered magneto-mechano-triboelectric nanogenerator enabled by reliable pattern replication for self-powered IoT devices, Sustain. Energy Fuels 8 (2024) 649–656, https://doi.org/10.1039/d3se01206a.

[35] H.S. Chen, Glassy metals, Rep. Prog. Phys. 43 (1980) 353, https://doi.org/10.1007/978-3-662-47882-0.

[36] J. Gutiérrez, J.M. Barandiarán, P. Mínguez, Z. Kaczkowski, P. Ruuskanen, G. Vlasák, P. Svec, P. Duhaj, Influence of heat treatment on the magnetic and piezomagnetic properties of amorphous and nanocrystalline Fe64Ni10Nb 3Cu1Si13B9 alloy strips, Sens. Actuators A Phys. 106 (2003) 69–72, https://doi.org/10.1016/S0924-4247(03)00136-5.

[37] M. Chen, Mechanical behavior of metallic glasses: microscopic understanding of strength and ductility, Annu. Rev. Mater. Res. 38 (2008) 445–469, https://doi.org/10.1146/annurev.matsci.38.060407.130226.

[38] M. Peddigari, K. Woo, S.D. Kim, M.S. Kwak, J.W. Jeong, J.H. Kang, S.H. Lee, J. H. Park, K. Il Park, V. Annapureddy, J. Jang, Y. Min, C.W. Ahn, J.J. Choi, B. D. Hahn, W.H. Yoon, J. Ryu, G.T. Hwang, Ultra-magnetic field sensitive magnetoelectric composite with sub-pT detection limit at low frequency enabled by flash photon annealing, Nano Energy 90 (2021): 106598, https://doi.org/10.1016/j.nanoen.2021.106598.

[39] Z. Chu, H. Shi, W. Shi, G. Liu, J. Wu, J. Yang, S. Dong, Enhanced resonance magnetoelectric coupling in (1-1) connectivity composites, Adv. Mater. 29 (2017) 1–9, https://doi.org/10.1002/adma.201606022.

[40] Z. Fang, S.G. Lu, F. Li, S. Datta, Q.M. Zhang, M. El Tahchi, Enhancing the magnetoelectric response of Metglas/polyvinylidene fluoride laminates by exploiting the flux concentration effect, Appl. Phys. Lett. 95 (2009) 1–4, https://doi.org/10.1063/1.3231614.

[41] M.E. McHenry, M.A. Willard, D.E. Laughlin, Amorphous and nanocrystalline materials for applications as soft magnets, Prog. Mater. Sci. 44 (1999) 291–433, https://doi.org/10.1016/S0079-6425(99)00002-X.

[42] A.H. Alameh, M. Gratuze, F. Nabki, Impact of geometry on the performance of cantilever-based piezoelectric vibration energy harvesters, IEEE Sens. J. 19 (2019) 10316–10326, https://doi.org/10.1109/JSEN.2019.2932341.

[43] I.C. Nlebedim, N. Ranvah, P.I. Williams, Y. Melikhov, J.E. Snyder, A.J. Moses, D. C. Jiles, Effect of heat treatment on the magnetic and magnetoelastic properties of cobalt ferrite, J. Magn. Magn Mater. 322 (2010) 1929–1933, https://doi.org/10.1016/j.jmmm.2010.01.009.

[44] M.J. PourhosseiniAsl, X. Gao, S. Kamalisiahroudi, Z. Yu, Z. Chu, J. Yang, H.Y. Lee, S. Dong, Versatile power and energy conversion of magnetoelectric composite materials with high efficiency via electromechanical resonance, Nano Energy 70 (2020): 104506, https://doi.org/10.1016/j.nanoen.2020.104506.

[45] S. Dong, J. Zhai, Equivalent circuit method for static and dynamic analysis of magnetoelectric laminated composites, Chin. Sci. Bull. 53 (2008) 2113–2123, https://doi.org/10.1007/s11434-008-0304-7.

[46] H. Song, J. Jang, M. Peddigari, S. Pattipaka, Y. Min, K. Il Park, C.K. Jeong, H.E. Lee, J.H. Park, H.Y. Lee, W.H. Yoon, J. Ryu, G.T. Hwang, Self-powered light dimming system using a magneto-mechano-electric generator with hardener-doped Pb(Mg1/3Nb2/3)O3-Pb(Zr,Ti)O3 single crystals, J. Mater. Chem. A Mater. 11 (2023) 3364–3372, https://doi.org/10.1039/d2ta06732c.

[47] H. Jabbar, H.J. Jung, N. Chen, D.H. Cho, T.H. Sung, Piezoelectric energy harvester impedance matching using a piezoelectric transformer, Sens. Actuators A Phys. 264 (2017) 141–150, https://doi.org/10.1016/j.sna.2017.07.036.